The Astrophysical Journal, 859:59 (10pp), 2018 May 20 https://doi.org/10.3847/1538-4357/aabc52

Constraining the Molecular Complexity in the Interstellar Medium—The Formation of Ethyl Methyl Ether ($CH_3OCH_2CH_3$) in Star-forming Regions

Alexandre Bergantini[1,2], Robert Frigge[1,2], and Ralf I. Kaiser[1,2]
[1] Department of Chemistry, University of Hawaii at Mānoa, Honolulu, HI 96822, USA; ralfk@hawaii.edu
[2] W.M. Keck Laboratory in Astrochemistry, University of Hawaii at Mānoa, Honolulu, HI 96822, USA
Received 2018 January 20; revised 2018 April 3; accepted 2018 April 4; published 2018 May 23

Abstract

We report the first confirmed synthesis of ethyl methyl ether (EME, $CH_3CH_2OCH_3$) within astrophysical model ices containing water (H_2O) and methane (CH_4) exposed to ionizing radiation at ultra-low temperatures of 5 K. EME (also known as methoxyethane), was recently observed toward Orion KL and currently is the largest confirmed oxygen-bearing molecule found in the interstellar medium. Exploiting isomer-selective photoionization (PI) of the subliming molecules in the temperature-programmed desorption phase at 10.49, 9.92, and 9.70 eV, coupled with reflectron time-of-flight mass spectrometry and isotopic substitution experiments ($H_2^{18}O$–CH_4), the detection of fragment ions of EME at $m/z = 45$ ($C_2H_5O^+$) and $m/z = 59$ ($C_3H_7O^+$), and probing the proton transfer in subliming ethanol–EME complexes via $m/z = 61$ ($C_3H_9O^+$), the present study reveals that EME can be formed from suprathermal reactions initiated by cosmic rays and secondary electrons generated within astrophysical ices. The detection of EME in our experiments represents a significant advance in the understanding of formation pathways of complex organic molecules present in hot cores and helps to constrain astrochemical models on the formation of such species within molecular clouds.

Key words: astrochemistry – cosmic rays – infrared: general – ISM: molecules – methods: laboratory: solid state – radiation mechanisms: non-thermal

1. Introduction

As the size and detection sensitivity of telescopes increase (Jørgensen et al. 2012; Tercero et al. 2013), significant attention from experimental and observational astrophysicists has been devoted to the detection and elucidation of the formation routes of complex organic molecules (COMs) in star-forming regions (Müller et al. 2016). One of the recent achievements in this field is the observation of ethyl methyl ether (EME; $CH_3OCH_2CH_3$) toward Orion KL (Tercero et al. 2015), a molecule whose presence in the interstellar medium (ISM) has been theorized and pursued for the last decades (Charnley et al. 2001, 1995; Fuchs et al. 2003, 2005; Carroll et al. 2015). Charnley et al. (2001) searched for EME in Orion KL, W51 e1/e2, and Sgr B2(N), proposing a detection toward the hot core W51 e1/e2; this assignment was based on three torsionally unresolved lines and hence was disputed by Fuchs et al. (2005) and by Carroll et al. (2015). Fuchs et al. (2005) searched for EME toward the hot core regions G34.26, NGC 6334(I), Orion KL, and W51 e1/e2 using the IRAM 30 m and the SEST 15 m telescopes; although these authors proposed the detection of EME toward W51 e1/e2, this study was subsequently contested by Carroll et al. (2015). Carroll et al. (2015) also failed in detecting EME toward W51 e1/e2 using the 12 m Telescope of the Arizona Radio Observatory and toward the high-mass star-forming region Sgr B2(N-LMH) exploiting the Green Bank 100 m Telescope. Finally, Tercero et al. (2015), using the IRAM 30 m telescope and the ALMA Science Verification (SV) data, detected 46 unblended lines of EME and reported its detection toward Orion KL. So far, the work of Tercero et al. has not been disputed, and it represents the best confirmed detection of EME in the ISM.

Previous models (Charnley et al. 2001, 1995; Fuchs et al. 2003, 2005; Carroll et al. 2015) suggested that EME is likely to be present in hot cores within dense molecular clouds as a result of unstudied gas-phase ion-molecule reactions involving methanol (CH_3OH) and ethanol (C_2H_5OH) sublimed from the surface of interstellar grains, as the temperature rises to a range of 100–300 K during the process of high-mass star formation (Reactions (1)–(3)). This is conjectured to eventually form EME through dissociative recombination with electrons (Reaction 4):

$$CH_3OH + H_3^+ \rightarrow CH_3OH_2^+ + H_2, \quad (1a)$$

$$CH_3OH + H_3O^+ \rightarrow CH_3OH_2^+ + H_2O, \quad (1b)$$

$$CH_3OH + HCO^+ \rightarrow CH_3OH_2^+ + CO, \quad (1c)$$

$$CH_3OH_2^+ + C_2H_5OH \rightarrow C_2H_5OH_2^+ + CH_3OH, \quad (2)$$

$$C_2H_5OH_2^+ + CH_3OH \rightarrow C_2H_6OCH_3^+ + H_2O, \quad (3)$$

$$C_2H_6OCH_3^+ \xrightarrow{e^-} C_2H_5OCH_3 + H. \quad (4)$$

This model (Reactions (1)–(4)) predicts that hot cores with initial ethanol abundances of 10^{-6} and 10^{-7} with respect to hydrogen would lead to peak abundances of EME of the order of 10^{-9} and 10^{-10}, respectively, within 10^4 years after the sublimation of the grain mantles (Charnley et al. 1995). From models used to fit the data collected toward Orion KL by the ALMA interferometer, Tercero et al. (2015) estimated an upper limit for the trans-EME column density of $(4.0 \pm 0.8) \times 10^{15}$ cm^{-2} in that source. Future observations may provide additional data that will allow a direct comparison between the abundances estimated by gas-phase-dominated models at temperatures of 100–300 K (e.g., Charnley et al. 2001, 1995; Fuchs et al. 2003, 2005; Carroll et al. 2015), with the abundances predicted by cosmic-ray-driven, grain surface-dominated models, at lower temperatures ($T < 100$ K) (Abplanalp et al. 2016; Shingledecker & Herbst 2018), followed by sublimation of the synthesized EME when the

Table 1
Data Applied to Calculate the Irradiation Dose per Molecule in the H_2O/CH_4 Ice

Initial kinetic energy of the electrons, E_{init} (keV)[a]		5
Irradiation current, I (nA)[a]		96 ± 5
Total number of electrons[a]		$(2.15 \pm 0.22) \times 10^{15}$
Average penetration depth, l (nm)[a]		266 ± 52
Average kinetic energy of backscattered electrons, E_{bs} (keV)[a]		3.18 ± 0.32
Fraction of backscattered electrons, f_{bs}[a]		0.31 ± 0.10
Average kinetic energy of transmitted electrons, E_{trans} (keV)[a]		0
Fraction of transmitted electrons, f_{trans}[a]		0
Density of the ice, ρ (g cm^{-3})		0.92 ± 0.10
Irradiated area, A (cm^2)		1.0 ± 0.1
Dose (eV/molecule)	Water (H_2O)	(10.44 ± 1.25)
	Methane (CH_4)	(9.28 ± 1.11)

Note.
[a] Parameters obtained from CASINO software v2.42.

temperature of the grains increases to up to 300 K in the vicinity of a protostar (Pirronello et al. 1982; Bernstein et al. 1997; Ehrenfreund et al. 1997; Tielens 2009; Bergantini et al. 2017; Förstel et al. 2017).

Here, we report the first confirmed synthesis of EME within processed astrophysical model ices containing water and methane at ultra-low temperatures; based on these results we propose that EME can be first synthesized within interstellar grains in cold molecular clouds at temperatures around 10 K as a result of non-equilibrium reactions triggered by the interaction of cosmic rays with ice-coated interstellar grains, with subsequent sublimation of the molecules taking place in the vicinity of a protostar as the temperature of the grains increases. Investigation of the complex chemistry taking place in the irradiated water (H_2O)–methane (CH_4) ice samples was carried out with the support of three spectrometric techniques: online and in situ Fourier transform infrared spectroscopy (FTIR) of the ice samples, electron-impact quadrupole mass spectrometry operating in residual gas analyzer mode (EI-QMS/RGA), and the recently established fragment-free tunable vacuum-ultraviolet (VUV) photoionization reflectron time-of-flight mass spectrometry (PI-ReTOF-MS) of the subliming molecules (Turner et al. 2015; Abplanalp & Kaiser 2017; Bergantini et al. 2017, 2018; Förstel et al. 2017; Góbi et al. 2017, 2018; Tarczay et al. 2017; Tsegaw et al. 2017; Abplanalp et al. 2018). Although FTIR has been extensively used to characterize astrophysical model ices in previous laboratory simulation experiments, in multiple instances, due to overlapping fundamentals of the newly formed molecules, it does not allow the identification of individual COMs, but only functional groups at best (Bergantini et al. 2014; Abplanalp et al. 2016). The universal EI-QMS/RGA can effectively detect gas-phase species, but the fragmentation caused by the 70 eV electrons utilized to ionize the molecules often results in significant fragmentation and hence in a convoluted spectrum, thus it is not always a suitable method to reliably identify COMs in those studies (Kaiser et al. 1995a, 1995b). Moreover, previous experiments have demonstrated that the EI-QMS/RGA is not sensitive enough to detect low-yield products, e.g., (Bergantini et al. 2017; Förstel et al. 2017). Therefore, the detection of EME in our studies was exclusively possible by exploiting tunable VUV PI-ReTOF-MS along with isotopically labeled reactants, so that the detection of distinct structural isomers with different ionization energies could be resolved (Jones & Kaiser 2013; Kaiser et al. 2015; Bergantini et al. 2018). The detection of EME in our experiments represents a significant advance in the understanding of formation pathways of COMs found in hot cores, and helps to constrain astrochemical models on the formation of such species within molecular clouds and hot cores.

Table 2
Ice Composition and Photoionization Energies Exploited in the Experiments

Ice Composition	Tunable VUV Energy (eV)	Average Flux ($\times 10^{12}$ Photons s^{-1})
H_2O/CH_4	10.49	2.6 ± 0.5
H_2O/CH_4	9.92	1.7 ± 0.2
H_2O/CH_4	9.70	1.3 ± 0.2
$H_2^{18}O/CH_4$	10.49	1.9 ± 0.4
$H_2^{18}O/CH_4$	9.92	1.3 ± 0.2

2. Experimental Methods

The experiments were carried out in a contamination-free stainless steel ultra-high-vacuum chamber (UHV) evacuated to a base pressure of a few 10^{-11} Torr. Ice mixtures were prepared via deposition of water–methane gas mixtures onto a polished silver (Ag) coupled to a cold finger, cooled at temperatures of 5.5 ± 0.2 K using a closed-cycle helium cryostat (Sumitomo Heavy Industries, RDK-415E). The compounds used in the experiment—water (H_2O, Fischer Chemical, HPLC grade; $H_2^{18}O$, Sigma-Aldrich, 99% atom ^{18}O; methane (CH_4, 99.999%, Specialty Gases of America)—were premixed in a gas mixing chamber (GMC) kept at pressures of a few 10^{-8} Torr. The water samples were degassed through several freeze-pump-thaw cycles before introducing them into the GMC. The (9 ± 1) to 1 water–methane ratio (nominally 9 to 1) was achieved by introducing partial pressures of 18.1 ± 0.3 Torr of water and 1.2 ± 0.1 Torr of methane in the GMC prior to each deposition. The water–methane ratio of the mixture was determined via separate calibration experiments using a calibrated quadrupole mass spectrometry operating in residual gas analyzer mode (QMS-RGA) with 70 eV electrons as described in Bergantini et al. (2017). Each gas mixture (H_2O–CH_4, $H_2^{18}O$–CH_4) was deposited using a glass capillary array held 30 ± 5 mm in front of the silver substrate for 540 ± 30 s at pressures $(2.0 \pm 0.5) \times 10^{-8}$ Torr in the main chamber. The ice growth was monitored online and in situ by measuring the interference pattern (fringes) produced by a 632.8 nm HeNe laser (CVI Melles Griot; 25-LHP-230) as the laser beam was being reflected off the substrate into a photodiode interfaced to a picoammeter (Keithley 6485). The ice thickness of 700 ± 50 nm was calculated using the methodology described by Turner et al. (2015) and Bergantini et al. (2017), exploiting a refractive index for the ice mixtures of 1.30 ± 0.03 (Satorre et al. 2008; Luna et al. 2012). Each ice sample was then irradiated by 5 keV electrons at (96 ± 5) nA of current for one hour at an angle of 70° relative to the surface normal of the substrate, which, based on CASINO simulations (Drouin et al. 2007), and using the parameters described in Table 1, yields a dose of (10.44 ± 1.25) eV per water molecule and (9.28 ± 1.11) eV per methane molecule. These doses are equivalent to $(3 \pm 0.5) \times 10^7$ yr of exposure to galactic

Table 3
Infrared Absorption Features Recorded before and after the Irradiation of Water/Methane (H_2O/CH_4)

Absorptions Before Irradiation (cm^{-1})	Absorptions After Irradiation (cm^{-1})	Assignment	Carrier	References
4299		$\nu_3 + \nu_4$ (CH_4)	combination	Hodyss et al. (2009)
4203		$\nu_1 + \nu_4$ (CH_4)	combination	Hodyss et al. (2009)
3849		$3\nu_4$ (CH_4)	overtone	Bennett et al. (2006) Ennis et al. (2011)
3717, 3688, 3657		H_2O	dangling O–H bond	Zondlo et al. (1997)
3245		ν_1 (H_2O)	O–H stretch	d'Hendecourt & Allamandola (1986) Gerakines et al. (1995)
3008		ν_3 (CH_4)	degenerate stretch	Hodyss et al. (2009)
	2975	ν_{10} (C_2H_6)	CH_2 symmetric stretch/CH_3 degenerate stretch/CH_3 asymmetric stretch	Kaiser et al. (2014)
		$\nu_{as}(C_3H_8)$		Abplanalp & Kaiser (2016)
	2941	$\nu_8 + \nu_{11}$ (C_2H_6)	combination	Boudin et al. (1998)
	2882	ν_5 (C_2H_6)	CH_3 stretch	Zhou et al. (2014)
	2831	ν_3 (CH_3OH)	C–H stretch	Wen et al. (1998)
2903		ν_1 (CH_4)	symmetric stretch	Hodyss et al. (2009)
2817		$\nu_2 + \nu_4$ (CH_4)	combination	Hodyss et al. (2009) Abplanalp & Kaiser (2016)
2595		$2\nu_4$ (CH_4)		Hodyss et al. (2009)
	2341	ν_3 (CO_2)	C=O asymmetric stretch	Oancea et al. (2012) Bergantini et al. (2014)
1659		ν_2 (H_2O)	O–H bend	d'Hendecourt & Allamandola (1986)
1301		ν_4 (CH_4)	degenerate deformation	Hodyss et al. (2009) Abplanalp & Kaiser (2016)
	1125	ν_7 (CH_3OH)	CH_3 rock	Wen et al. (1998)
	1045	alcohol*	CH_3 deformation, C–C stretch, C–C–O stretch	Tong et al. (2010) Schriver et al. (2007) Plyler (1952)
	1014	ν_8 (CH_3OH)	C–O stretch	Wen et al. (1998) Bennett et al. (2007)
800		ν_R (H_2O)	H_2O libration	d'Hendecourt & Allamandola (1986)

cosmic rays in the interior of a typical molecular cloud (Yeghikyan 2011), which is about the same as the lifetime of a molecular cloud (Blitz & Shu 1980; Larson 1981).

After the irradiation, the sample is kept isothermally at (5.5 ± 0.2) K for one hour to check the stability and reactivity of the molecular species generated within the ice sample before the beginning of the temperature-programmed desorption (TPD) phase. The TPD consists of warming-up the sample from 5.5 to 300 K at 0.5 K $minute^{-1}$ rate, during which the subliming molecules are continuously probed by PI-ReTOF-MS (Jordan TOF Products, Inc.) using a multichannel plate in dual chevron configuration. The signal is amplified by a fast preamplifier (Ortec 9305) and shaped with a 100 MHz discriminator. The resulting spectrum is recorded by a personal-computer-based-multichannel scalar (FAST ComTec, P7888-1 E) with a bin width of 4 ns, triggered at 30 Hz by a signal generator (Quantum Composers, 9518). The ReTOF-MS produces 3600 sweeps per mass spectrum every two minutes. The soft photoionization of the molecules is rendered with pulsed (30 Hz) coherent VUV photons. Experiments exploiting natural and isotopically labeled molecules and VUV photons with energies of 10.49 eV (118.19 nm), 9.92 eV (125.00 nm), and 9.70 eV (127.80 nm) were required to resolve the signal of EME from structural isomers and from molecules holding the same molecular mass, i.e., C_3H_8O and $C_2H_4O_2$ isomers (Table 2). The process of the generation of VUV light is described in detail by Bergantini et al. (2017), so it will be mentioned here only briefly. The 10.49 eV (118.22 nm) light was produced via the third harmonic (354.6 nm) of a Nd:YAG laser (Spectra-Physics, PRO-250-30; 325 mJ $pulse^{-1}$) via frequency tripling ($\omega_{vuv} = 3\omega_1$) in pulsed jets of xenon as nonlinear medium. The 9.92 eV light was generated by a resonant four-wave mixing ($\omega_{vuv} = 2\omega_1 - \omega_2$) process in which a beam (ω_1), generated by the second harmonic (532 nm, 2.330 eV) of the fundamental of a Nd:YAG laser (Spectra-Physics, PRO-270-30; 600 mJ $pulse^{-1}$) was converted to 606.948 nm (2.043 eV) with the use of a dye laser (Sirah Lasertechnik, model Cobra-Stretch), and then frequency-tripled (202.316 nm; 6.128 eV) using two β-BaB_2O_4 (BBO) crystals at 44° and 77°, was combined with a 532 nm (2.33 eV) beam generated by a different Nd:YAG laser (Spectra-Physics, PRO-250-30; 550 mJ $pulse^{-1}$) inside a chamber where pulsed jets of krypton acted as a nonlinear medium. Finally, the 9.92 eV photons were generated by combining the $\omega_1$202.316 nm (6.128 eV) photons with ω_2 484.98 nm (2.55 eV) photons also in krypton as a nonlinear medium; in this case, the 484.98 nm

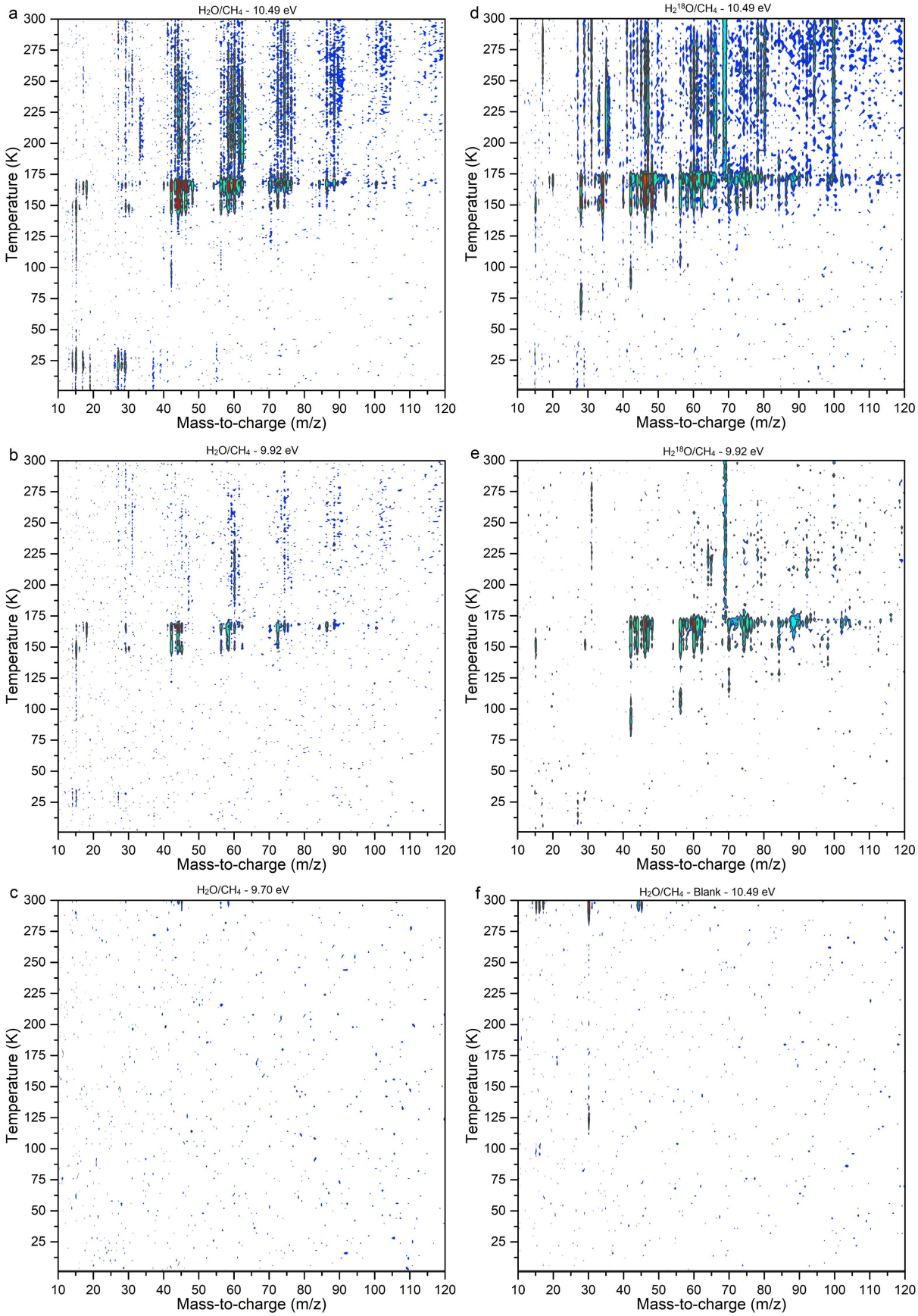

Figure 1. PI-ReTOF-MS data recorded in the H_2O/CH_4 and $H_2^{18}O/CH_4$ experiments: (a) H_2O/CH_4 (PI = 10.49 eV), (b) H_2O/CH_4 (PI = 9.92 eV), (c) H_2O/CH_4(PI = 9.70 eV), (d) $H_2^{18}O/CH_4$ (PI = 10.49 eV), (e) $H_2^{18}O/CH_4$(PI = 9.92 eV), and (f) H_2O/CH_4 (PI = 10.49 eV) (blank).

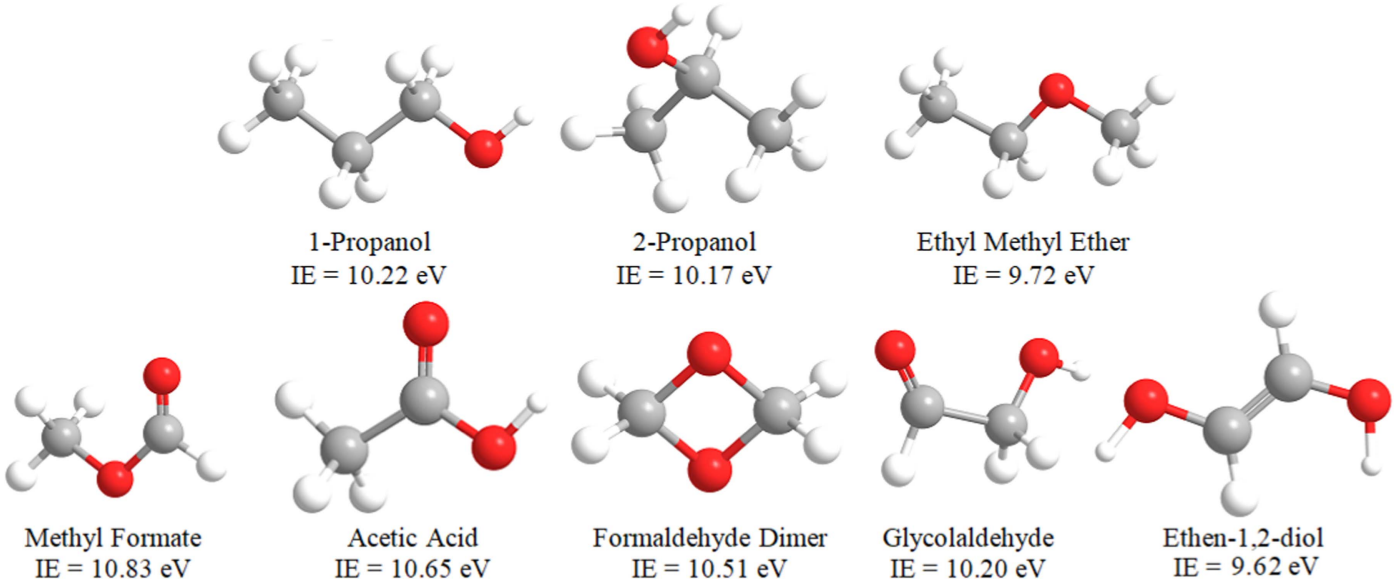

Figure 2. Molecular structures of isomers of C_3H_8O (top row) and $C_2H_4O_2$(bottom row), along with their ionization energies in eV.

photons were produced by pumping 354.6 nm light in a dye laser (Sirah Lasertechnik, model Precision Scan) using Coumarin 480 dye. The flux of VUV photons (Table 2) was measured using a photodiode (Opto Diode Corp.; model SXUV100) calibrated by the National Institute of Standards and Technology (NIST).

3. Results and Discussion

3.1. FTIR

The water–methane samples were monitored via FTIR before and during the irradiation phase of the experiment to keep track of the irradiation-induced modifications on the ice. These modifications are observed as a decrease of the IR bands of the reactants, as well as the emergence of novel absorption bands corresponding to the products. As depicted in Table 3, the spectrum of the irradiated H_2O–CH_4 ice reveals absorptions of ethane (C_2H_6) and/or propane (C_3H_8) at 2975 cm^{-1}, 2941 cm^{-1}, and 2882 cm^{-1} (Bennett et al. 2006; Hodyss et al. 2009; Abplanalp et al. 2015). Absorptions linked to methanol (CH_3OH) can be observed at 2831, 1125, and 1014 cm^{-1} (Bennett et al. 2007; Bergantini et al. 2014; Maity et al. 2014). The 2341 cm^{-1} absorption originates from carbon dioxide (Bennett et al. 2010; Oancea et al. 2012). Finally, a new peak at 1045 cm^{-1} is characteristic of alcohols (Plyler 1952; Moore & Hudson 2005; Schriver et al. 2007; Tong et al. 2010). According to Durig et al. (2002), the most intense bands of solid EME in the mid-infrared region are the CH_3 antisymmetric stretch at 2972 cm^{-1}, the CH_3 symmetric deformation at 1394 cm^{-1}, the CH_3(O) in-plane rock at 1212 cm^{-1}, and the COC antisymmetric and symmetric stretches at 1115 cm^{-1} and 852 cm^{-1}, respectively. The $H_2^{18}O$–CH_4ices support these assignments, demonstrating isotopic shifts by the heavier ^{18}O atom by up to 38 cm^{-1} (Bergantini et al. 2017). Considering that our experiments were carried out at relatively low doses, concentrations of EME are too low to be observed spectroscopically via FTIR. The same applies to common species such as formaldehyde (H_2CO), which was observed in similar studies on the photolysis of water–methane ices by Hodyss et al. (2009), but not in our experiments. Finally, we concluded that even though FTIR represents an optimal tool to investigate the processing and decay kinetics of small interstellar species such as carbon monoxide (CO), water (H_2O), methanol (CH_3OH), carbon dioxide (CO_2), and methane (CH_4), this approach is limited when the investigation of larger species—such as COMs—is necessary, since many of the IR spectral features of complex molecules may be overlapped (Abplanalp et al. 2016; Bergantini et al. 2014).

3.2. PI-ReTOF-MS Data

After irradiation, during the warm-up phase, the subliming products were monitored via PI-ReTOF-MS using distinct PI energies in different experiments, so the molecules of interest could be selectively ionized and detected depending on each case. The complete PI-ReTOF-MS data recorded for the H_2O–CH_4 and $H_2^{18}O$–CH_4 systems is compiled in Figure 1, which reveals the ion signal as a function of temperature from 5 to 300 K, with mass-to-charge ratios displayed from $m/z = 10$ to $m/z = 120$. Figures 1(a)–(c) depict the data from the H_2O–CH_4 system at photoionization energies of 10.49 eV, 9.92 eV, and 9.70 eV, respectively; Figures 1(d) and (e) show the data from the $H_2^{18}O$–CH_4 system at PI energies of 10.49 eV and 9.92 eV, respectively. The data of the blank experiment—i.e., an experiment carried out at identical conditions, but without the irradiation of the H_2O–CH_4 ice by energetic electrons—are displayed in Figure 1(f) (PI = 10.49 eV). Note that Figure 1 shows multiple simultaneous counts in the 145–170 K interval. Rather than being the result of the fragmentation of large molecules, these simultaneous counts occur because most of the products are trapped in the amorphous water ice matrix, being released only after the beginning of water desorption, as observed by Jenniskens & Blake (1994) and in recent similar experiments by e.g., Bergantini et al. (2014, 2017) and Jones et al. (2014).

Here, we focus on the detection of ethyl methyl ether ($CH_3OCH_2CH_3$; C_3H_8O; IE = 9.72 ± 0.07 eV; Bowen & Maccoll 1984) along with its structural isomers at $m/z = 60$: *1-propanol* (IE = 10.22 ± 0.06 eV; Bowen & Maccoll 1984), *2-propanol* (IE = 10.17 ± 0.02 eV; Bowen & Maccoll 1984). An ion signal at $m/z = 60$ may be also associated with the

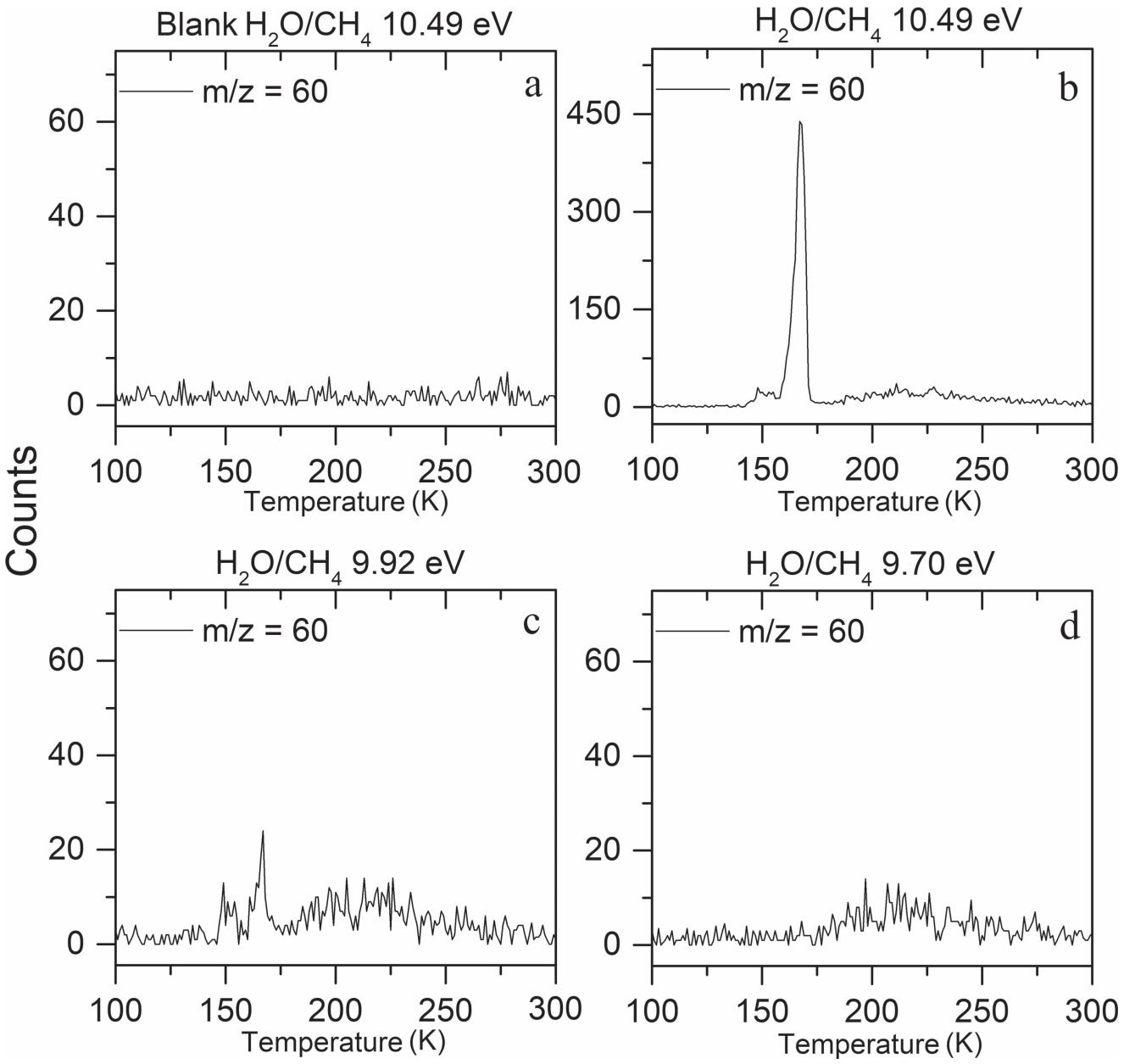

Figure 3. TPD profile corresponding to $m/z = 60$ (C_3H_8O and $C_2H_4O_2$ isomers) as collected during (a) the blank experiment at 10.49 eV and from the irradiated samples during the TPD phases at (b) 10.49 eV, (c) 9.92 eV, and (d) 9.70 eV.

molecular formula $C_2H_4O_2$: *methyl formate* (IE = 10.83 ± 0.02 eV; Waterstradt et al. 1994), *acetic acid* (IE = 10.65 ± 0.02 eV; Knowles & Nicholson 1974), *glycolaldehyde* (IE = 10.20 ± 0.02 eV; Maity et al. 2014), and *ethene-1,2-diol* (IE = 9.62 ± 0.04 eV; Tureček & Havlas 1986) (Figure 2).

The TPD profiles extracted for $m/z = 60$ in the H_2O–CH_4systems are compiled in Figure 3 for distinct photoionization energies from 10.49 to 9.70 eV. Based solely on the photoionization energy, the signal detected at PI = 10.49 eV (Figure 3(b)) could be linked to any of the C_3H_8O isomers (1-propanol, 2- propanol, ethyl methyl ether) or to two $C_2H_4O_2$ isomers (glycolaldehyde, ethene-1,2-diol); methyl formate and acetic acid cannot be ionized since their ionization energies of 10.83 eV and 10.65 eV are above the energy of the photons utilized here (10.49 eV). Three desorption profiles are present: a sharp event at 150 K, an intense and narrow sublimation event peaking at 170 K, and a broad sublimation event from 180 K to about 250 K with ion counts lower by a factor of 15. By decreasing the photon energy to 9.92 eV (Figure 3(c)), only ethyl methyl ether and ethene-1,2-diol can be photoionized, since all other isomers have ionization energies above 9.92 eV. All three sublimation events are still visible, with the first and third events having peak ion counts about half of the intensity of the third sublimation event at 170 K. Lowering the photon energy to 9.70 eV (Figure 3(d)) eliminates the early sublimation events peaking at 150 and 170 K; the TPD profile of the third sublimation event from 180 K to about 250 K is still present. Therefore, considering the aforementioned ionization energies, we can conclude that the sublimation events peaking at 150 and 170 K are linked to the formation of ethyl methyl ether ($CH_3OCH_2CH_3$; C_3H_8O), whereas the broad sublimation events are connected to ethene-1,2-diol (OHCHCHOH; $C_2H_4O_2$). This sublimation sequence also correlated with an

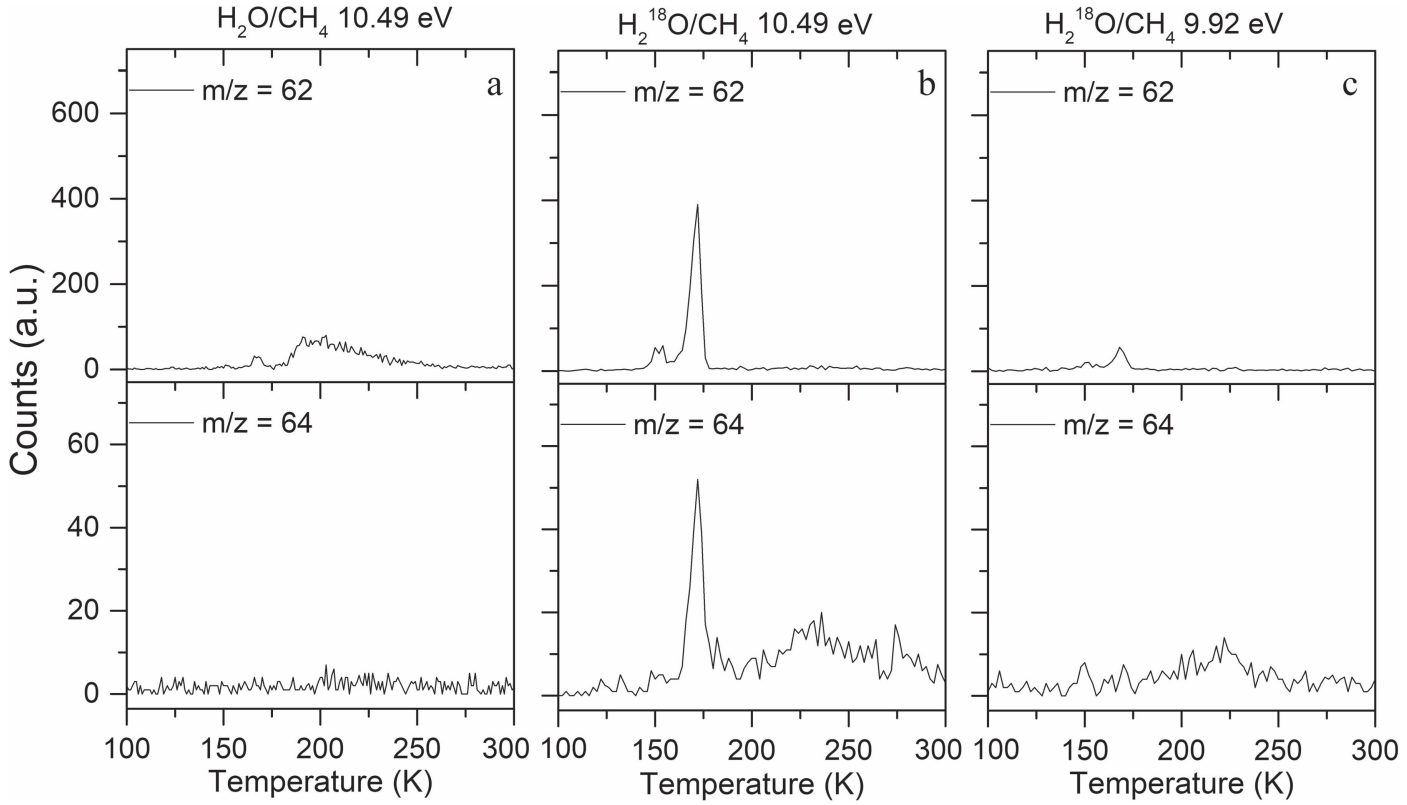

Figure 4. TPD profiles recorded at $m/z = 62$ and $m/z = 64$ in the H_2O/CH_4 and $H_2^{18}O/CH_4$ systems.

enhanced polarity of ethene-1,2-diol compared to ethyl methyl ether and the dominance of strong hydrogen bonding compared to weaker dipole–dipole interactions, respectively. Finally, the absence of any signal at $m/z = 60$ in the blank experiment verifies that signal detected in the irradiation experiments originates from the processing of the ice samples, excluding the possibility that the unprocessed reactants can directly produce any of the species detected at $m/z = 60$.

To substantiate the identification of ethyl methyl ether, experiments utilizing isotopic labeled ices were also performed ($H_2^{18}O$–CH_4) so the signal from C_3H_8O isomers (60 amu) could be detached from $C_2H_4O_2$ (60 amu) isomers based on their mass-shifts to 62 amu ($C_3H_8^{18}O$) and 66 amu ($C_2H_4^{18}O_2$). Figure 4 compiles the TPD profiles extracted for $m/z = 62$ and 64 comparing the H_2O–CH_4 with $H_2^{18}O$–CH_4systems at two distinct photon energies of 10.49 eV and 9.92 eV. First, Figure 4(a) reveals that a small signal at $m/z = 62$ was present in the H_2O–CH_4 experiment; this signal could be assigned to dimethyl peroxide ($(CH_3O)_2$) or to methoxymethanol (CH_3OCH_2OH). In this case, this signal shifts from $m/z = 62$ to $m/z = 66$, which is detectable in the $H_2^{18}O$–CH_4 experiment, but not in the H_2O–CH_4 system. This finding confirms that the signal at $m/z = 62$ in the H_2O–CH_4 system belongs to dimethyl peroxide $(CH_3O)_2$ and/or methoxymethanol (CH_3OCH_2OH) and that the signal at $m/z = 62$ in the $H_2^{18}O$–CH_4 experiment must originate from a different species, i.e., the $C_3H_8^{18}O$ isomer ethyl methyl ether subliming at 170 K, which can be ionized at 10.49 and 9.92 eV. On the other hand, the signal at $m/z = 64$ is completely absent in the H_2O–CH_4 experiment (Figure 4(a)), suggesting that in the $H_2^{18}O$–CH_4 system (Figures 4(b) and (c)), $C_2H_4^{18}O_2$ isomers, i.e., ethene-1,2-diol ($H^{18}OCHCH^{18}OH$), with the signal being barely visibly at 9.92 eV. Note that a small fraction of close to 10% of ethene-1,2-diol co-sublimes with the ethyl methyl ether ($CH_3^{18}OCH_2CH_3$). It is important to note that the fragmentation patterns of alkenes, aromatic hydrocarbons, alcohols, phenols, ethers, ketones, aldehydes, and esters, do not produce signals at $m/z = 60$. On the other hand, some carboxylic acids do fragment at $m/z = 60$, but the appearance energy of these fragments is above 9.92 eV, which is the case for fragments from butanoic acid (AE = 10.45 eV), pentanoic acid (AE = 10.8 eV), hexanoic acid (AE = 10.52 eV), and heptanoic acid (AE = 10.54 eV). Higher-order carboxylic acids are not detected in our experiments.

Having elucidated the formation of EME in the H_2O–CH_4 system based on isotopic substitution studies (^{18}O) and selective photoionization of distinct C_3H_8O–$C_3H_8^{18}O$ isomers, we provide additional evidence based on unique fragmentation patterns of EME. If the photoionization of a molecule is carried out close to the ionization energy, little internal energy is available in the $C_3H_8O^+$ parent ion to fragment. Therefore, photoionization is often characterized as a fragment-free (soft) ionization technique. However, as the energy of the photon increases, the internal energy in the $C_3H_8O^+$ parent ion rises as well; this enhanced internal energy might lead to a characteristic fragmentation of the $C_3H_8O^+$ parent ion at distinct appearance energies (AE). In the case of EME, $C_2H_5O^+$ ($m/z = 45$; AE = 10.7 eV) and $C_3H_7O^+$ ($m/z = 59$; AE = 10.3 eV) (Bowen & Maccoll 1984) represent characteristic fragment ions. Likewise, the signal at $m/z = C_3H_9O^+(m/z = 61)$ could originate from a proton transfer within subliming ethanol–EME complexes (Figure 5; Lam et al. 2004).

We can also provide quantitative information on the production yields of ethyl methyl ether ($CH_3OCH_2CH_3$) and how they compare to dimethyl ether (CH_3OCH_3). Accounting

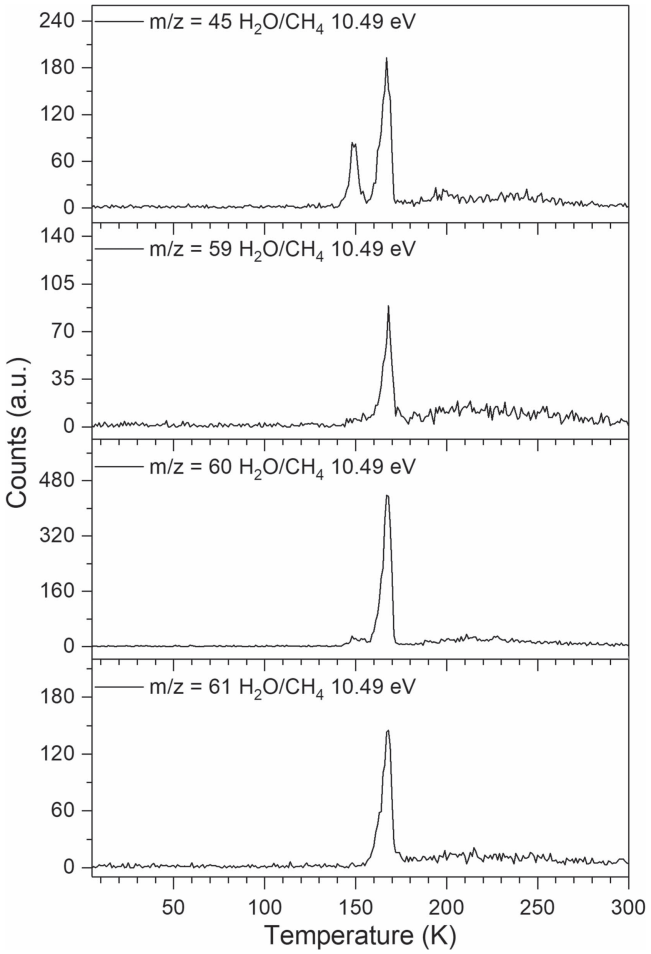

Figure 5. TPD profiles of fragment ions of EME at $m/z = 45$ ($C_2H_5O^+$) and $m/z = 59$ ($C_3H_7O^+$) recorded at photoionization energies of 10.49 eV in the H_2O/CH_4 system. We suggest that the signal at $m/z = 61$ ($C_3H_9O^+$) originates from proton transfer in subliming ethanol–EME complexes. The TPD of EME ($m/z = 60$) is plotted for comparison. Sublimation events associated with EME are peaking close to 170 K.

for the flux of the photons at 10.49 eV in the photoionization experiment (Table 2), and the photoionization cross section of ethyl methyl ether of 10.71×10^{-18} cm^2 at 10.49 eV (Koizumi 1991), we can derive yields of $(6.2 \pm 1.5) \times 10^{-4}$ ethyl methyl ether molecules eV^{-1}. This results in a ratio of dimethyl ether (CH_3OCH_3) to ethyl methyl ether ($CH_3OCH_2CH_3$) of 2.6 ± 0.3: 1 in our experiments, i.e., a dominating fraction of dimethyl ether (CH_3OCH_3). The yields were calculated using the methodology described by Bergantini et al. (2017, 2018). In brief, calibration experiments in which a known amount of gas was deposited on the substrate, followed by a regular TPD, were performed. By varying the thickness of the ice samples and cross-referencing the FTIR, QMS/RGA, and ReTOF-MS data with the flux of VUV photons and the ionization cross section of the studied molecular species, we were able to find, within a margin of error, a correlation between the spectroscopic data and the actual number of molecules produced in the sample due to the processing of the ice.

4. Astrophysical Implications

Having provided compelling evidence of the first detection of ethyl methyl ether ($CH_3OCH_2CH_3$) and of [^{18}O]-ethyl methyl ether ($CH_3^{18}OCH_2CH_3$) in laboratory simulation experiments mimicking the exposure of interstellar model ices containing water and methane to ionizing radiation at 5 K, we now discuss possible formation pathways (Figure 6). A detailed analysis of the molecular structure of ethyl methyl ether ($CH_3OCH_2CH_3$), along with a retrosynthetic approach (Bennett et al. 2005), identifies three pathways via simple bond-rupture processes and four mechanisms via insertion of suprathermal species. Let us have a close look at the simple bond-rupture processes. The ethyl methyl ether holds three chemically non-equivalent carbon–carbon and carbon–oxygen single bonds, whose hemolytic bond ruptures lead to three radical pairs: methyl ($CH_3\cdot$) plus methoxymethyl ($\cdot CH_2OCH_3$) (*rad1*), ethyl ($CH_3CH_2\cdot$) plus methoxy ($CH_3O\cdot$) (*rad2*), and ethoxy ($CH_3CH_2O\cdot$) plus methyl ($CH_3\cdot$) (*rad3*). These in turn can be generated in ices containing methane (CH_4)–dimethyl ether (CH_3OCH_3), ethane (C_2H_6)–methanol (CH_3OH), and ethanol (CH_3CH_2OH)–methane (CH_4), respectively. Alternatively, four barrierless insertion processes (*ins1-ins4*) can lead to ethyl methyl ether via insertion of singlet carbene (CH_2; a^1A_1) into any of the six carbon–hydrogen bonds of dimethyl ether (CH_3OCH_3) (*ins1*), into the carbon-oxygen bond of dimethyl ether (CH_3OCH_3) (*ins2*), or into the hydrogen-oxygen bond of ethanol (CH_3CH_2OH) (*ins4*); finally, insertion of electronically excited oxygen ($O(^1D)$) into the carbon–carbon single bond of propane ($CH_3CH_2CH_3$) could form ethyl methyl ether (*ins3*). Note that carbene can be generated via interaction of ionizing radiation such as galactic cosmic rays (Kaiser & Roessler 1998) or energetic electrons with methane (CH_4)

Which are the most likely precursor molecules? It is important to note that none of the seven systems as discussed above have been detected on icy grains; propane ($CH_3CH_2CH_3$), as required for mechanism *ins3,* represents a second-generation hydrocarbon product formed in the radiolysis of methane from ethane (CH_3CH_3) and methane (CH_4), respectively. Furthermore, insertion of ($O(^1D)$) into the screened and hence sterically less accessible carbon–carbon bond of propane, is less likely compared to insertion into accessible carbon–hydrogen bonds of propane leading to 1- and 2-propanol (C_3H_7OH)—structural isomers of ethyl methyl ether. However, the present experiments do not provide any evidence on the formation of these alcohols, therefore we can likely exclude propane ($CH_3CH_2CH_3$) as a precursor to ethyl methyl ether. The remaining systems require the presence of ethanol (CH_3CH_2OH)–methane (CH_4) (*rad3, ins4*), dimethyl ether (CH_3OCH_3)–methane (CH_4) (*rad1, ins1, ins2*), and ethane (C_2H_6)–methanol (CH_3OH), (*rad2*) precursors in the ices. A recent investigation of the interaction of ionizing radiation with methanol–methane ices led to the detection of ethanol (CH_3CH_2OH) and dimethyl ether (CH_3OCH_3) with branching ratios of (2.33 ± 0.14) : 1 (Bergantini et al. 2018). Therefore, successive reactions of these primary reaction products ethanol and dimethyl ether, with methane involving the aforementioned radical–radical and/or carbene-insertion reactions, are likely pathways to synthesize ethyl methyl ether in irradiated ices, thus classifying ethyl methyl ether as a "second-generation" ether formed via stepwise molecular growth processes involving methyl radicals or carbene-insertion sequences. These molecular mass growth processes have been observed recently in the (D3)-nitromethane ices subjected to energetic electrons (Tsegaw et al. 2016).

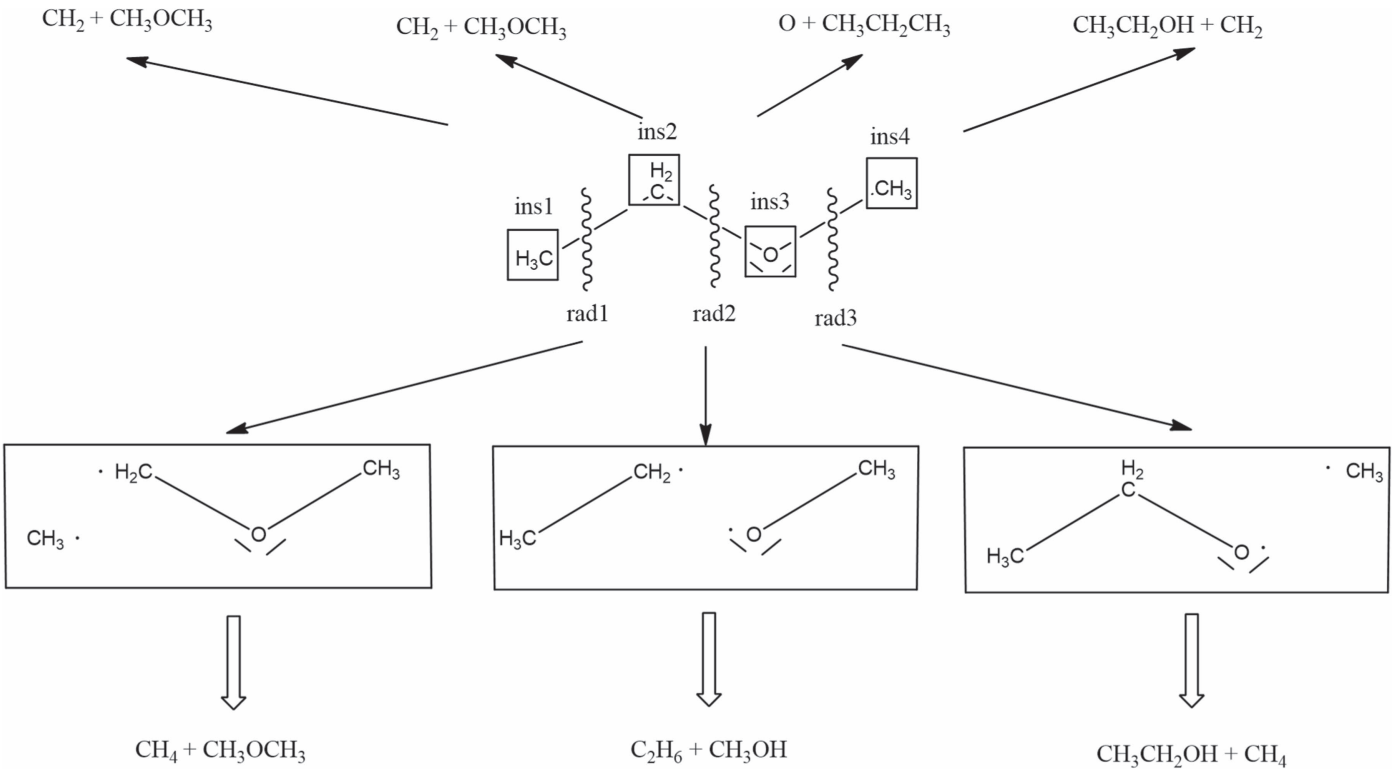

Figure 6. Retrosynthetic pathways on the formation of ethyl methyl ether via radical–radical (bottom) and insertion reactions (top).

Finally, it is important to highlight the energetics involved in the formation of ethyl methyl ether. Here, the overall formation from methane and water requires 16.1 eV (Reaction (5)). Accounting for the elemental reaction steps, Bergantini et al. (2017) demonstrated that the synthesis of ethanol (CH_3CH_2OH) and dimethyl ether (CH_3OCH_3) in methanol (CH_3OH)–methane (CH_4) ices requires initial carbon–hydrogen and oxygen–hydrogen bond-rupture processes that are endoergic by 4.3 and 4.5 eV, respectively. Oxygen–hydrogen bond cleavages in dimethyl ether (CH_3OCH_3) and ethanol (CH_3CH_2OH) necessary for reaction sequences *rad1* and *rad3*, respectively, require 4.20 eV (Good & Francisco 1997) and 4.55 eV (Matus et al. 2007) (Reactions (6) and (7)) with subsequent radical–radical reactions that are exoergic by 3.79 and 3.62 eV, respectively (Reactions (8) and (9)). Analysis of the energetics of the aforementioned reaction sequences underlines the need of non-equilibrium processes initiated by energy transfer processes from the ionizing radiation within the low-temperature ices to transfer the energy to the reactants and hence exclude the possibility of a thermal synthesis of ethyl methyl ether in these ices:

$$3CH_4 + H_2O \rightarrow CH_3CH_2OCH_3 + 6H, \quad (5)$$

$$CH_3OCH_3 \rightarrow CH_3OCH_2 \cdot + H, \quad (6)$$

$$CH_3CH_2OH \rightarrow CH_3CH_2O \cdot + H, \quad (7)$$

$$CH_3OCH_2 \cdot + CH_3 \cdot \rightarrow CH_3CH_2OCH_3, \quad (8)$$

$$CH_3CH_2O \cdot + CH_3 \cdot \rightarrow CH_3CH_2OCH_3. \quad (9)$$

Since dimethyl ether (CH_3OCH_3) *and* ethyl methyl ether ($CH_3OCH_2CH_3$) have been observed toward Orion KL, the experimentally derived dimethyl ether (CH_3OCH_3) to ethyl methyl ether ($CH_3OCH_2CH_3$) ratio of 2.6 ± 0.3: 1 supports the concept of stepwise molecular mass growth processes of ethyl methyl ether ($CH_3OCH_2CH_3$), *at least* from dimethyl ether (CH_3OCH_3). Therefore, we can conclude that dimethyl ether (CH_3OCH_3), and possibly its ethanol isomer (CH_3CH_2OH), are central precursors involved in the synthesis of ethyl methyl ether ($CH_3OCH_2CH_3$) on interstellar grains through a facile non-equilibrium chemistry (Figure 6), which delivers the required energy by the impinging ionizing radiation, and therefore the missing reaction pathways to ethyl methyl ether ($CH_3OCH_2CH_3$) as observed toward Orion KL. Our data and the diminished abundance of ethyl methyl ether ($CH_3OCH_2CH_3$), compared to dimethyl ether (CH_3OCH_3), lead to the prediction that further molecular mass growth processes may lead to more complex ethers such as diethyl ether ($CH_3CH_2OCH_2CH_3$) or methyl propyl ether ($CH_3OC_3H_7$), with C_3H_7defining the n- or isopropyl group. These higher molecular mass ethers are expected to reveal an even lower abundance compared to ethyl methyl ether ($CH_3OCH_2CH_3$) compared to dimethyl ether (CH_3OCH_3). Considering that no complex organics carrying two ethyl groups or a methyl and propyl group in the same molecule have been detected this far, the prospective identification of diethyl ether ($CH_3CH_2OCH_2CH_3$) or methyl propyl ether ($CH_3OC_3H_7$) would be essential for refining contemporary astrochemical models of molecular clouds and of hot cores, thus bringing us closer to an understanding of the synthesis of COMs in the universe. Note that the contribution of gas-phase chemistry in the formation of EME in the ISM requires detailed chemical modeling, therefore it is not accounted for in the present study and should be investigated in future projects.

We thank the US National Science Foundation (AST-1505502) for support in conducting the present experiments.

The authors acknowledge the W. M. Keck Foundation for financing the experimental setup.

ORCID iDs

Alexandre Bergantini https://orcid.org/0000-0003-2279-166X
Ralf I. Kaiser https://orcid.org/0000-0002-7233-7206

References

Abplanalp, M., Jones, B., & Kaiser, R. I. 2018, PCCP, 20, 5435
Abplanalp, M. J., Borsuk, A., Jones, B. M., & Kaiser, R. I. 2015, ApJ, 814, 45
Abplanalp, M. J., Förstel, M., & Kaiser, R. I. 2016, CPL, 644, 79
Abplanalp, M. J., Gozem, S., Krylov, A. I., et al. 2016, PNAS, 113, 7727
Abplanalp, M. J., & Kaiser, R. I. 2016, ApJ, 827, 132
Abplanalp, M. J., & Kaiser, R. I. 2017, ApJ, 836, 195
Bennett, C. J., Chen, S-H., Sun, B-J., Chang, A. H. H., & Kaiser, R. I. 2007, ApJ, 660, 1588
Bennett, C. J., Jamieson, C. S., & Kaiser, R. I. 2010, PCCP, 12, 4032
Bennett, C. J., Jamieson, C. S., Osamura, Y., & Kaiser, R. I. 2005, ApJ, 624, 1097
Bennett, C. J., Jamieson, C. S., Osamura, Y., & Kaiser, R. I. 2006, ApJ, 653, 792
Bergantini, A., Góbi, S., Abplanalp, M. J., & Kaiser, R. I. 2018, ApJ, 852, 70
Bergantini, A., Maksyutenko, P., & Kaiser, R. I. 2017, ApJ, 841, 96
Bergantini, A., Pilling, S., Nair, B. G., Mason, N. J., & Fraser, H. J. 2014, A&A, 570, A120
Bernstein, M. P., Allamandola, L. J., & Sandford, S. A. 1997, AdSpR, 19, 991
Blitz, L., & Shu, F. H. 1980, ApJ, 238, 148
Boudin, N., Schutte, W. A., & Greenberg, J. M. 1998, A&A, 331, 749
Bowen, R. D., & Maccoll, A. 1984, JMSp, 19, 379
Carroll, P. B., McGuire, B. A., Blake, G. A., et al. 2015, ApJ, 799, 15
Charnley, S., Ehrenfreund, P., & Kuan, Y.-J. 2001, AcSpA, 57, 685
Charnley, S., Kress, M. E., Tielens, A. G. G. M., & Millar, T. J. 1995, ApJ, 448, 232
d'Hendecourt, L. B., & Allamandola, L. 1986, A&AS, 64, 453
Drouin, D., Couture, A. R., Joly, D., et al. 2007, Scanning, 29, 92
Durig, J. R., Jin, Y., Phan, H. V., Liu, J., & Durig, D. T. 2002, Struct. Chem., 13, 1
Ehrenfreund, P., Boogert, A. C. A., Gerakines, P. A., Tielens, A. G. G. M., & van Dishoeck, E. F. 1997, A&A, 328, 649
Ennis, C., Yuan, H., Sibener, S. J., & Kaiser, R. I. 2011, PCCP, 13, 17870
Förstel, M., Bergantini, A., Maksyutenko, P., Góbi, S., & Kaiser, R. I. 2017, ApJ, 845, 83
Fuchs, G. W., Giesen, T. F., & Wyrowski, F. 2005, A&A, 444, 521
Fuchs, U., Winnewisser, G., Groner, P., De Lucia, F. C., & Herbst, E. 2003, ApJS, 144, 277
Gerakines, P. A., Schutte, W. A., Greenberg, J. M., & van Dishoeck, E. F.. 1995, A&A, 296, 810
Góbi, S., Bergantini, A., Turner, A. M., & Kaiser, R. I. 2017, JPCA, 121, 3879
Góbi, S., Zhao, L., Xu, B., et al. 2018, CPL, 691, 250
Good, D., & Francisco, J. 1997, CPL, 266, 512
Hodyss, R., Johnson, P. V., Stern, J. V., Goguen, J. D., & Kanik, I. 2009, Icar, 200, 338
Jenniskens, P., & Blake, D. F. 1994, Sci, 265, 753
Jones, B. M., & Kaiser, R. I. 2013, J. Phys. Chem. Lett., 4, 1965
Jones, B. M., Kaiser, R. I., & Strazzulla, G. 2014, ApJ, 781, 85
Jørgensen, J. K., Favre, C., Bisschop, S. E., et al. 2012, ApJL, 757, L4
Kaiser, R. I., Gabrysch, A., & Roessler, K. 1995, RScI, 66, 3058
Kaiser, R. I., Jansen, P., Petersen, K., & Roessler, K. 1995, RScI, 66, 5226
Kaiser, R. I., Maity, S., & Jones, B. M. 2014, PCCP, 16, 3399
Kaiser, R. I., Maity, S., & Jones, B. M. 2015, Angew. Chem. Int. Ed. Engl., 127, 197
Kaiser, R. I., & Roessler, K. 1998, ApJ, 503, 959
Knowles, D., & Nicholson, A. 1974, JChPh, 60, 1180
Koizumi, H. 1991, JChPh, 95, 5846
Lam, S., Shi, Y. J., Mosey, N. J., Woo, T. K., & Lipson, R. H. 2004, JChPh, 121, 10006
Larson, R. B. 1981, MNRAS, 194, 809
Luna, R., Satorre, M. Á., Domingo, M., Millán, C., & Santonja, C. 2012, Icar, 221, 186
Maity, S., Kaiser, R. I., & Jones, B. M. 2014, FaDi, 168, 485
Matus, M. H., Nguyen, M. T., & Dixon, D. A. 2007, JPCA, 111, 113
Moore, M. H., & Hudson, R. L. 2005, in Proc. IAU Symp. 231, Astrochemistry: Recent Successes and Current Challenges, ed. D. C. Lis et al. (Cambridge: Cambridge Univ. Press), 247
Müller, H. S., Belloche, A., Xu, L. H., et al. 2016, A&A, 587, A92
Oancea, A., Grasset, O., Le Menn, E., et al. 2012, Icar, 221, 900
Pirronello, V., Brown, W. L., Lanzerotti, L. J., Marcantonio, K. J., & Simmons, E. H. 1982, ApJ, 262, 636
Plyler, E. K. 1952, JRNBS, 48
Satorre, M., Domingo, M., Millán, C., et al. 2008, P&SS, 56, 1748
Schriver, A., Schriver-Mazzuoli, L., Ehrenfreund, P., & d'Hendecourt, L. 2007, CP, 334, 128
Shingledecker, C. N., & Herbst, E. 2018, PCCP, 20, 5359
Tarczay, G., Förstel, M., Góbi, S., Maksyutenko, P., & Kaiser, R. I. 2017, Chem. Phys. Chem., 18, 882
Tercero, B., Cernicharo, J., López, A., et al. 2015, A&A, 582, L1
Tercero, B., Kleiner, I., Cernicharo, J., et al. 2013, ApJL, 770, L13
Tielens, A. G. G. M. 2009, in Astrophysics in the Next Decade (Berlin: Springer), 271
Tong, H.-J., Yu, J. Y., Zhang, Y. H., & Reid, J. P. 2010, JPCA, 114, 6795
Tsegaw, Y. A., Góbi, S., Förstel, M., et al. 2017, JPCA, 121, 7477
Tsegaw, Y. A., Sander, W., & Kaiser, R. I. 2016, JPCA, 120, 1577
Tureček, F., & Havlas, Z. 1986, J. Chem. Soc. Perkin., 2, 1011
Turner, A. M., Abplanalp, M. J., Chen, S. Y., et al. 2015, PCCP, 17, 27281
Waterstradt, E., Jung, R., Belling, T., & Müller-Dethlefs, K. 1994, BBGPC, 98, 176
Wen, A. T., Michaud, M., & Sanche, L. 1998, JESRP, 94, 23
Yeghikyan, A. 2011, Ap, 54, 87
Zhou, L., Maity, S., Abplanalp, M., Turner, A., & Kaiser, R. I. 2014, ApJ, 790, 38
Zondlo, M. A., Onasch, T. B., Warshawsky, M. S., et al. 1997, JPCB, 101, 10887